22

Linear and Nonlinear Optical Properties of Ferroelectric Thin Films

Bing Gu and Hui-Tian Wang
School of Physics, Nankai University
China

1. Introduction

Nowadays, nonlinear optical materials play a crucial role in the technology of photonics, nano-photonics, and bio-photonics. Among a wide variety of materials, thin films have the additional design advantage of small volume and good compatibility with fabrication of waveguide and integrated nonlinear photonics devices over solutions and single crystals.

Interestingly, most ferroelectric thin films exhibit notable physical characteristics of large spontaneous polarization, high dielectric constant, high optical transparency, and large nonlinear response with respect to the electromagnetic radiation in the optical range. During the past decade, ferroelectric thin films such as $Bi_2Nd_2Ti_3O_{12}$, $Ba_{0.6}Sr_{0.4}TiO_3$, and $Bi_{3.25}La_{0.75}Ti_3O_{12}$ have been received intense interest due to their high optical transparency and remarkable optical nonlinearity for potential applications on nonlinear photonic devices (Gu et al., 2004, Liu et al., 2006, Shi et al., 2006, Shin et al., 2007). Moreover, most of these investigations have been performed under the excitation of nanosecond and picosecond laser pulses. Owing to today's fast advance of laser sources with ultrashort pulse duration, the femtosecond nonlinear optical response has been detected in several ferroelectric thin films. Enlightened by a recent report on the third-order nonlinear optical response presented in $CaCu_3Ti_4O_{12}$ at a wavelength of 532 nm (Ning et al., 2009), observations indicate that the optical nonlinearities depend strongly on the pulse duration of the excitation laser, although many reports declared that the observed nonlinear effect is an instantaneous optical nonlinearity in the nanosecond and picosecond regimes. Apparently, it is imperative to gain an insight on the underlying physical mechanisms for the observed optical nonlinearities at different time scales.

In this chapter, the linear transmittance spectrum and Z-scan technique are used to characterize the linear and nonlinear optical properties of ferroelectric thin films, respectively. Two methodologies are based on measurements of the sample's transmittance under weak or intense light excitation. The nonlinear optical properties of representative ferroelectric films in nanosecond, picosecond, and femtosecond regimes are presented. In particular, the underlying mechanisms for the observed optical nonlinearities are also discussed in details.

2. Concept of linear and nonlinear optics

The interaction of light with matter will modify either the direction of propagation, spatial profile, or transmission of an applied optical field through a material system. The

fundamental parameter in this light-matter interaction theory is the electric polarization of the material induced by light. In the case of conventional (i.e., linear) optics, the polarization depends linearly upon the electric field strength in a manner that can often be written as

$$\vec{P} = \varepsilon_0 \chi^{(1)} \cdot \vec{E} \,, \tag{1}$$

where the constant of proportionality $\chi^{(1)}$ is the linear susceptibility and ε_0 is the permittivity of free space. In an isotropic medium, the real and imaginary parts of $\chi^{(1)}$ in SI units, respectively, are related to the linear index of refraction and absorption coefficient by

$$n_0 = \sqrt{1 + \mathrm{Re}[\chi^{(1)}]} \,, \tag{2}$$

$$\alpha_0 = \frac{\omega}{n_0 c} \mathrm{Im}[\chi^{(1)}] \,. \tag{3}$$

Here c is the speed of light in vacuum and ω is the optical frequency. The refractive index of ferroelectric films is attributed to the following factors which are related to the crystallinity of the film density, electronic structure, and defects. Owning to high dielectric constant, generally, the index of refraction in the ferroelectric film is over 2 in the visible region. The linear absorption coefficient of materials usually contains the contributions of two parts: one is the elastic scattering caused by the defects and optical inhomogeneity and another is the inherent linear absorption. In general, the linear absorption coefficient of ferroelectric thin films is close to 10^4 cm^{-1}. The main reason is that the elastic scattering is the dominant factor to the linear absorption (Gu et al., 2004, Leng et al., 2007). Typical values of n_0 and α_0 of representative ferroelectric thin films are listed in Tables 1 and 2.

In nonlinear optics, nonlinear processes are responsible for the nonlinearity of materials. Accordingly, the polarization induced by the applied optical field in the material system can be expressed as a power series in the electric field amplitude (Boyd, 2009):

$$\vec{P} = \varepsilon_0 \chi^{(1)} \cdot \vec{E} + \varepsilon_0 \chi^{(2)} : \vec{E}\vec{E} + \varepsilon_0 \chi^{(3)} \vdots \vec{E}\vec{E}\vec{E} + \cdots \,. \tag{4}$$

The quantities $\chi^{(2)}$ and $\chi^{(3)}$ are called the second- and third-order nonlinear optical susceptibilities of the sample, respectively. The theoretical formalism has been presented for the calculation of nonlinear susceptibilities components in ferroelectrics (Murgan et al., 2002). Generally, the nonlinear susceptibilities depend on the frequencies of the applied light fields, but under the assumption of instantaneous response, one takes them to be constants. The $\chi^{(2)}$ related nonlinear processes include second-harmonic generation, optical rectification, and sum- and difference-frequency generation. Such processes are out of the scope of this book chapter. More details with respect to second-order optical nonlinearities in ferroelectrics can be found elsewhere (Murgan et al., 2002, Tsai et al., 2004, Kumar et al., 2008, Kityk et al., 2010). The coefficient $\chi^{(3)}$ describes the intensity-dependent third-order nonlinear effect, such as self-focusing or defocusing, two-photon absorption, and three-harmonic generation. The intensity-dependent refractive index n_2 and absorption coefficient α_2 are most two important of all third-order processes in ferroelectrics, which are related to the real and imaginary components of $\chi^{(3)}$ in SI units, respectively, by (Chen et al., 2006)

$$n_2 = \frac{3\,\mathrm{Re}[\chi^{(3)}]}{4\varepsilon_0 c n_0^2}, \tag{5}$$

$$\alpha_2 = \frac{3\pi\,\mathrm{Im}[\chi^{(3)}]}{2\varepsilon_0 c n_0^2 \lambda}, \tag{6}$$

where n_2 and α_2 take the units of m^2/W and m/W, respectively. And λ is the wavelength of laser in vacuum.

3. Physical mechanisms of optical nonlinearities in ferroelectric thin films

Optical nonlinear response of the ferroelectric thin film partly depends on the laser characteristics, in particular, on the laser pulse duration and on the excitation wavelength, and partly on the material itself. The optical nonlinearities usually fall in two main categories: the instantaneous and accumulative nonlinear effects. If the nonlinear response time is much less than the pulse duration, the nonlinearity can be regarded justifiably as responding instantaneously to optical pulses. On the contrary, the accumulative nonlinearities may occur in a time scale longer than the pulse duration. Besides, the instantaneous nonlinearity (for instance, two-photon absorption and optical Kerr effect) is independent of the the laser pulse duration, whereas the accumulative nonlinearity depends strongly on the pulse duration. Examples of such accumulative nonlinearities include excited-state nonlinearity, thermal effect, and free-carrier nonlinearity. The simultaneous accumulative nonlinearities and inherent nonlinear effects lead to the huge difference of the measured nonlinear response on a wide range of time scales.

3.1 Nonlinear absorption

In general, nonlinear absorption in ferroelectric thin films can be caused by two-photon absorption, three-photon absorption, or saturable absorption. When the excitation photon energy and the bandgap of the film fulfil the multiphoton absorption requirement [$(n-1)h\nu<E_g<nh\nu$] (here n is an integer. n=2 and 3 for two- and three-photon absorption, respectively), the material simultaneous absorbs n identical photons and promotes an electron from the ground state of a system to a higher-lying state by virtual intermediate states. This process is referred to a one-step n-photon absorption and mainly contributes to the absorptive nonlinearity of most ferroelectric films. When the excitation wavelength is close to the resonance absorption band, the transmittance of materials increases with increasing optical intensity. This is the well-known saturable absorption. Accordingly, the material has a negative nonlinear absorption coefficient.

3.2 Nonlinear refraction

The physical mechanisms of nonlinear refraction in the ferroelectric thin films mainly involve thermal contribution, optical electrostriction, population redistribution, and electronic Kerr effect. The thermal heat leads to refractive index changes via the thermal-optic effect. The nonlinearity originating from thermal effect will give rise to the negative nonlinear refraction. In general, the thermal contribution has a very slow response time (nanosecond or longer). On the picosecond and femtosecond time scales, the thermal contribution to the change of the refractive index can be ignored for it is much smaller than the electronic contribution. Optical

electrostriction is a phenomenon that the inhomogeneous optical field produces a force on the molecules or atoms comprising a system resulting in an increase of the refractive index locally. This effect has the characteristic response time of nanosecond order. When the electron occurs the real transition from the ground state of a system to a excited state by absorbing the single photon or two indential photons, electrons will occupy real excited states for a finite period of time. This process is called a population redistribution and mainly contributes the whole refractive nonlinearity of ferroelectric films in the picosecond regime. The electronic Kerr effect arises from a distortion of the electron cloud about atom or molecule by the optical field. This process is very fast, with typical response time of tens of femtoseconds. The electronic Kerr effect is the main mechanism of the refractive nonlinearity in the femtosecond time scale.

3.3 Accumulative nonlinearity caused by the defect

For many cases, the observed absorptive nonlinearity of ferroelectric thin films is the two-photon absorption type process. Moreover, the measured two-photon absorption coefficient strongly depends on the laser pulse duration (see Table 1). This two-photon type nonlinearity originates from two-photon as well as two-step absorptions. The two-step absorption is attributed to the introduction of electronic levels within the energy bandgap due to the defects (Liu et al., 2006, Ambika et al., 2009, Yang et al., 2009).

The photodynamic process in ferroelectrics with impurities is illustrated in Fig. 1. Electrons in the ground state could be promoted to the excited state and impurity states based on two- and one-photon absorption, respectively. The electrons in impurity states may be promoted to the excited state by absorbing another identical photon, resulting in two-step two-photon absorption. At the same time, one-photon absorption by impurity levels populates new electronic state. This significant population redistribution produces an additional change in the refractive index, leading to the accumulative nonlinear refraction effect. This accumulative nonlinearity is a cubic effect in nature and strongly depends on the pulse duration of laser. Similar to the procedure for analyzing the excited-state nonlinearity induced by one- and two-photon absorption (Gu et al., 2008b and 2010), the effective third-order nonlinear absorption and refraction coefficients arising from the two-step two-photon absorption can be expressed as

$$\alpha_2^{\text{imp}} = \frac{\sigma_{\text{imp}}\alpha_0}{h\nu}\frac{\sqrt{2}}{\sqrt{\pi}\tau}\int_{-\infty}^{+\infty}\exp(-\frac{t^2}{\tau^2})\left\{\int_{-\infty}^{t}\exp(-\frac{t'^2}{\tau^2})\exp(\frac{t'-t}{\tau_{\text{imp}}})dt'\right\}dt\,, \tag{7}$$

$$n_2^{\text{imp}} = \frac{\eta_{\text{imp}}\alpha_0}{h\nu}\frac{\sqrt{2}}{\sqrt{\pi}\tau}\int_{-\infty}^{+\infty}\exp(-\frac{t^2}{\tau^2})\left\{\int_{-\infty}^{t}\exp(-\frac{t'^2}{\tau^2})\exp(\frac{t'-t}{\tau_{\text{imp}}})dt'\right\}dt\,. \tag{8}$$

Here σ_{imp} and η_{imp} are the effective absorptive and refractive cross-sections of the impurity state, respectively. τ is the half-width at e^{-1} of the maximum for the pulse duration of the Gaussian laser. And τ_{imp} is the lifetime of the impurity state.

4. Characterizing techniques to determine the films' linear and nonlinear optical properties

In general, the ferroelectric thin film is deposited on the transparent substrate. The fundamental optical constants (the linear absorption coefficient, linear refraction index, and bandgap energy) of the thin film could be determined by various methods, such as the

prism-film coupler technique, spectroscopic ellipsometry, and reflectivity spectrum measurement. Among these methods, the transmittance spectrum using the envelope technique is a simple straightforward approach. To characterize the absorptive and refractive nonlinearities of ferroelectric films, the single-beam Z-scan technique is extensively adopted.

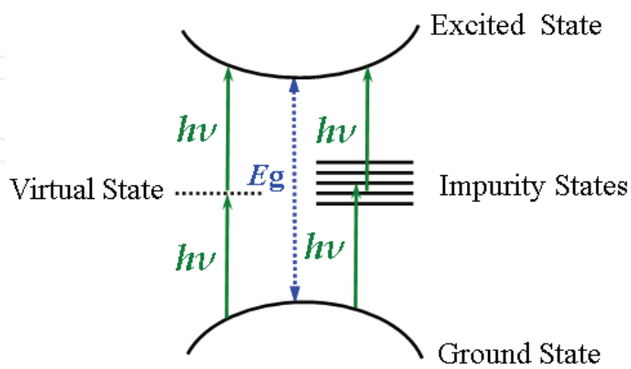

Fig. 1. Schematic diagram of one- and two-step two-photon absorption in ferroelectrics with the defects.

4.1 Linear optical parameters obtained from the transmittance spectrum using the envelope technique

The practical situation for a thin film on a thick finite transparent substrate is illustrated in Fig. 2. The film has a thickness of d, a linear refractive index n_0, and a linear absorption coefficient α_0. The transparent substrate has a thickness several orders of magnitude larger than d and has an index of refraction n_0^{sub} and an absorption coefficient $\alpha_0^{sub}\approx 0$. The index of the surrounding air is equal to 1.

Taking into account all the multiple reflections at the three interfaces, the rigorous transmission could be devised (Swanepoel, 1983). Subsequently, it is easy to simulate the transmittance spectrum from the given parameters (d, n_0, α_0, d^{sub}, and n_0^{sub}). The oscillations in the transmittance are a result of the interference between the air-film and film-substrate interface (for example, see Fig. 4). In contrast, in practical applications for determining the optical constants of films, one must employ the transmittance spectrum to evaluate the optical constants. The treatment of such an inverse problem is relatively difficult. From the measured transmittance spectrum, the extremes of the interference fringes are obtained (see dotted lines in Fig. 4). Based on the envelope technique of the transmittance spectrum, the optical constants (d, n_0, and α_0) could be estimated (Swanepoel, 1983).

The refractive index as a function of wavelength in the interband-transition region can be modelled based on dipole oscillators. This theory assumes that the material is composed of a series of independent oscillators which are set to forced vibrations by incident irradiances. Hereby, the dispersion of the refraction index is described by the well-known Sellmeier dispersion relation (DiDomenico & Wemple, 1969):

$$n_0^2(\lambda) = 1 + \sum_{j=0}^{M} \frac{b_j \lambda^2}{\lambda^2 - \lambda_j^{\,2}}, \tag{9}$$

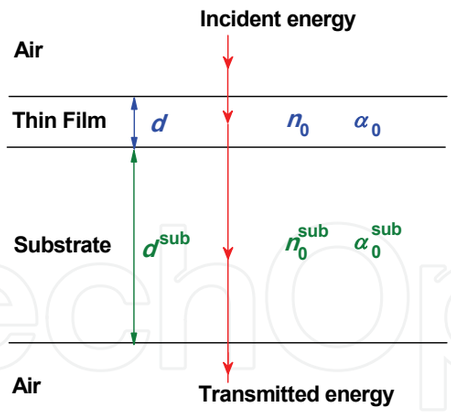

Fig. 2. Thin film on a thick finite transparent substrate.

where λ_j is the resonant wavelength of the jth oscillator of the medium, and b_j is the oscillator strength of the jth oscillator. In general, one assumes that only one oscillator dominates and then takes the one term of Eq. (9). This single-term Sellmeier relation fits the refractive index quite well for most materials. In some cases, however, to accurate describe the refractive index dispersion in the visible and infrared range, the improved Sellmeier equation which takes two or more terms in Eq. (9) is needed (Barboza & Cudney, 2009). Analogously, replacing n_0 by α_0 in Eq. (9), this equation describes the dispersion of linear absorption coefficient (Wang et al., 2004, Leng et al., 2007). In this instance, the parameters of λ_j and b_j have no special physical significance.

The optical bandgap (E_g) of the thin film can be estimated using Tauc's formula $(\alpha_0 h\nu)^{2/m}$=Const.$(h\nu\text{-}E_g)$, where $h\nu$ is the photon energy of the incident light, m is determined by the characteristics of electron transmitions in a material (Tauc et al., 1966). Here m=1 and 4 correspond the direct and indirect bandgap materials, respectively.

4.2 Z-scan technique for the nonlinear optical characterization

To characterize the optical nonlinearities of ferroelectric thin films, a time-averaging technique has been extensively exploited in Z-scan measurements due to its experimental simplicity and high sensitivity (Sheik-Bahae et al., 1990). This technique gives not only the signs but also the magnitudes of the nonlinear refraction and absorption coefficients.

4.2.1 Basic principle and experimental setup

On the basis of the principle of spatial beam distortion, the Z-scan technique exploits the fact that a spatial variation intensity distribution in transverse can induce a lenslike effect due to the presence of space-dependent refractive-index change via the nonlinear effect, affect the propagation behaviour of the beam itself, and generate a self-focusing or defocusing effect. The resulting phenomenon reflects on the change in the far-field diffraction pattern.

To carry out Z-scan measurements, the sample is scanned across the focus along the z-axis, while the transmitted pulse energies in the presence or absence of the far-field aperture is probed, producing the closed- and open-aperture Z-scans, respectively. The characteristics of the closed- and open-aperture Z-scans can afford both the signs and the magnitudes of the nonlinear refractive and absorptive coefficients. Figures 3(a) and 3(b) schematically show the closed- and open-aperture Z-scan experimental setup, respectively.

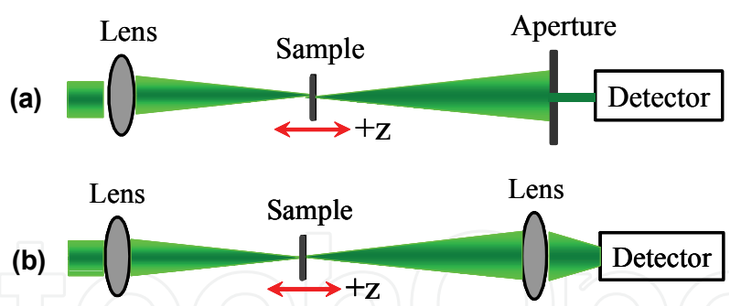

Fig. 3. Experimental setup of the (a) closed-aperture and (b) open-aperture Z-scan measurements.

In this book chapter, the nonlinear-optical measurements were conducted by using conventional Z-scan technique as shown in Fig. 3. The laser source was a Ti: sapphire regenerative amplifier (Quantronix, Tian), operating at a wavelength of 780 nm with a pulse duration of τ_F=350 fs (the full width at half maximum for a Gaussian pulse) and a repetition rate of 1 kHz. The spatial distribution of the pulses was nearly Gaussian, after passing through a spatial filter. Moreover, the laser pulses had near-Gaussian temporal profile, confirming by the autocorrelation signals in the transient transmission measurements. In the Z-scan experiments, the laser beam was focused by a lens with a 200 mm focal length, producing the beam waist at the focus ω_0≈31 μm (the Rayleigh range z_0=3.8 mm). To perform Z-scans, the sample was scanned across the focus along the z-axis using a computer-controlled translation stage, while the transmitted pulse energies in the present or absence of the far-field aperture were probed by a detector (Laser Probe, PkP-465 HD), producing the closed- and open-aperture Z-scans, respectively. For the closed-aperture Z-scans, the linear transmittance of the far-field aperture was fixed at 15% by adjusting the aperture radius. The measurement system was calibrated with carbon disulfide. In addition, neither laser-induced damage nor significant scattering signal was observed from our Z-scan measurements.

4.2.2 Z-scan theory for characterizing instantaneous optical nonlinearity

Assuming that the nonlinear response of the sample has a characteristic time much shorter than the duration of the laser pulse, i.e., the optical nonlinearity responds instantaneously to laser pulses. As a result, one can regard that the nonlinear effect depends on the instantaneous intensity of light inside the samples and each laser pulse is treated independently. For the sake of simplicity, we consider an optically thin sample with a third-order optical nonlinearity and the incoming pulses with a Gaussian spatiotemporal profile. The open-aperture Z-scan normalized transmittance can be expressed as

$$T(x,s=1)=\sum_{m=0}^{\infty}\frac{(-q_0)^m}{(x^2+1)^m(m+1)^{3/2}} \qquad \text{for } |q_0|<1\,. \tag{10}$$

where $x=z/z_0$ is the relative sample position, $q_0=\alpha_2 I_0(1\text{-}R)L_{\text{eff}}$ is the on-axis peak phase shift due to the absorptive nonlinearity, $L_{\text{eff}}=[1\text{-}\exp(\text{-}\alpha_0 L)]/\alpha_0$ is the effective sample length. Here z_0 is the Rayleigh length of the Gaussian beam; I_0 is the on-axis peak intensity in the air; R is the Fresnel reflectivity coefficient at the interface of the material with air; s is the linear transmittance of the far-field aperture; and L is the sample physical length.

The Z-scan transmittance for the pinhole-aperture is deduced as (Gu et al., 2008a)

$$T(x,s\approx 0)=1+\frac{1}{\sqrt{2}}\frac{4x\phi_0-(x^2+3)q_0}{(x^2+1)(x^2+9)}+\frac{1}{\sqrt{3}}\frac{4\phi_0^2(3x^2-5)+q_0^2(x^4+17x^2+40)-8\phi_0 q_0 x(x^2+9)}{(x^2+1)^2(x^2+9)(x^2+25)}, \quad (11)$$

where $\phi_0=2\pi n_2 I_0(1-R)L_{\mathrm{eff}}/\lambda$ is the on-axis peak nonlinear refraction phase shift. It should be noted that Eq. (11) is applicable to Z-scans induced by laser pulses with weak nonlinear absorption and refraction phase shifts. For arbitrary nonlinear refraction phase shift ϕ_0 and arbitrary aperture s, the Z-scan analytical expression is available in literature (Gu et al., 2008a).

4.2.3 Z-scan theory for a cascaded nonlinear medium

Ferroelectric thin film with good surface morphology was usually deposited on the quartz substrate by pulsed laser deposition, chemical-solution deposition, or radio-frequency magnetron sputtering. Generally, the thicknesses of the thin film and substrate are about sub-micron and millimetre, respectively. As shown in Fig. 2, the transparent substrate has a thickness three orders of magnitude large than that of the film. The quartz substrate has the nonlinear absorption coefficient of $\alpha_2^{\mathrm{sub}}\sim 0$ and the third-order refractive index of $n_2^{\mathrm{sub}}=3.26\times 10^{-7}$ cm^2/GW in the near infrared region (Gu et al., 2009a). The nonlinear refractive index of ferroelectric thin films in the femtosecond regime is usually three orders of magnitude larger than that of quartz substrate. Thus, the nonlinear optical path of the film ($n_2 L_{\mathrm{eff}} I_0$) is comparable with that of the substrate. In this instance, Z-scan signals arise from the resultant nonlinear response contributed by both the thin film and the substrate.

To separate each contribution, rigorous analysis should be adopted by the Z-scan theory for a cascaded nonlinear medium (Zang et al., 2003). Accordingly, the total nonlinear phase shifts due to the absorptive and refractive nonlinearities, q_0 and ϕ_0, could be extracted from the measured Z-scan experimental data for film/substrate. We can simplify q_0 and ϕ_0 as follows:

$$q_0 = I_0(1-R)[\alpha_2 L_{\mathrm{eff}} + (1-R')\alpha_2^{\mathrm{sub}} L_{\mathrm{eff}}^{\mathrm{sub}}], \quad (12)$$

$$\phi_0 = 2\pi I_0(1-R)[n_2 L_{\mathrm{eff}} + (1-R')n_2^{\mathrm{sub}} L_{\mathrm{eff}}^{\mathrm{sub}}]/\lambda\ . \quad (13)$$

Here $R=(n_0-1)^2/(n_0+1)^2$ and $R'=(n_0^{\mathrm{sub}}-n_0)^2/(n_0^{\mathrm{sub}}+n_0)^2$ are the Fresnel reflection coefficients at the air-sample and sample-substrate interfaces, respectively. Note that I_0 is the peak intensity just before the sample surface, whereas $I_0'=(1-R)I_0$ and $I_0''=(1-R')I_0'$ are the peak intensities within the sample and the substrate, respectively.

To unambiguously determine the optical nonlinearity of the thin film from the detected Z-scan signal, the strict approach is presented as follows (Gu et al., 2009a). Firstly, under the assumption that both the thin film and the substrate only exhibit third-order nonlinearities, the total nonlinear response of absorptive nonlinearity, q_0, and refractive nonlinearity, ϕ_0, are evaluated from the best fittings to the measured Z-scan traces for the composite system of thin film and substrate by using the Z-scan theory described subsection 4.2.2. Such evaluations are carried out for the Z-scans measured at different levels of I_0. Secondly, the nonlinear absorption α_2 and the nonlinear refraction index n_2 of the thin film can then be extracted from Eqs. (12) and (13). As such, the nonlinear coefficients of α_2 and n_2 for the thin

film at different values of I_0 are determined unambiguously and rigorously. Such the values of α_2 and n_2 as a function of I_0 provide a clue to the optical nonlinear origin of ferroelectrics.

4.2.4 Z-scan theory for the material with third- and fifth-order optical nonlinearities

Owing to intense irradiances of laser pulses, the higher-order optical nonlinearity has been observed in several materials, such as semiconductors, organic molecules, and ferroelectric thin films as we discussed in subsection 6.3.

For materials exhibiting the simultaneous third- and fifth-order optical nonlinearities, there is a quick procedure to evaluate the nonlinear parameters as follows (Gu et al., 2008b): (i) measuring the Z-scan traces at different levels of laser intensities I_0; (ii) determining the effective nonlinear absorption coefficient α_{eff} and refraction index n_{eff} of the film at different I_0 by using of the procedures described in subsections of 4.2.2 and 4.2.3; and (iii) fitting linearly the obtained α_{eff}~I_0 and n_{eff}~I_0 curves by the following equations

$$\alpha_{\text{eff}} = \alpha_2 + 0.544\alpha_3 I_0 , \tag{14}$$

$$n_{\text{eff}} = n_2 + 0.422 n_4 I_0 . \tag{15}$$

Here α_3 and n_4 are the fifth-order nonlinear absorption and refraction coefficients, respectively. If there is no fifth-order absorption effect, plotting α_{eff} as a function of I_0 should result in a horizon with α_2 being the intercept with the vertical axis. As the fifth-order absorption process presents, one obtains a straight line with an intercept of α_2 on the vertical axis and a slope of α_3. Analogously, by plotting n_{eff}~I_0, the non-zero intercept on the vertical axis and the slope of the straight line are determined the third- and fifth-order nonlinear refraction indexes, respectively. It should be emphasized that Eqs. (14) and (15) are applicable for the material exhibiting weak nonlinear signal.

5. Linear optical properties of polycrystalline $BiFeO_3$ thin films

The $BiFeO_3$ ferroelectric thin film was deposited on the quartz substrate at 650°C by radio-frequency magnetron sputtering. The relevant ceramic target was prepared using conventional solid state reaction method starting with high-purity (>99%) oxide powders of Bi_2O_3 and Fe_2O_3. It is noted that 10 wt % excess bismuth was utilized to compensate for bismuth loss during the preparation. During magnetron sputtering, the Ar/O_2 ratio was controlled at 7:1. The X-ray diffraction analysis demonstrated that the sample was a polycrystalline structure of perovskite phase. The observation from the scanning electron microscopy showed that the $BiFeO_3$ thin film and the substrate were distinctive and no evident inter-diffusion occurred between them.

The linear optical properties of the $BiFeO_3$ thin film were studied by optical transmittance measurements. The optical transmittance spectra of both the $BiFeO_3$ film on the quartz substrate and the substrate were recorded at room temperature with a spectrophotometer (Shimadzu UV-3600). The optical constants of the quartz substrate are d^{sub}=1 mm, n_0^{sub}=1.51, and $\alpha_0^{\text{sub}}\approx 0$. Accordingly, the transmission of the quartz is 0.92, in agreement with the experimental measurement (dashed line in Fig. 4). As displayed in Fig. 4, it is clear that the $BiFeO_3$ thin film is highly transparent with transmittance between 58% and 91% in the visible and near-infrared wavelength regions. The oscillations in the transmittance are a result of the interference between the air-film and film-substrate interface. The well-

oscillating transmittance indicates that the $BiFeO_3$ film has a flat surface and a uniform thickness. The transparency of the film drops sharply at 500 nm and the absorption edge is located at 450 nm. With these desired qualities, the $BiFeO_3$ thin film should be a promising candidate for applications in waveguide and photonic devices.

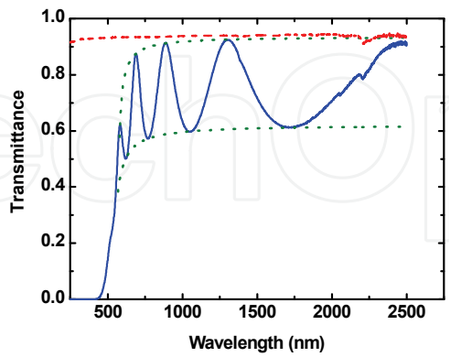

Fig. 4. Optical transmittance spectrum of $BiFeO_3$ thin film on a quartz substrate (solid line) and its envelope (dotted lines). For comparision, the result of quartz substrate is also presented (dashed line).

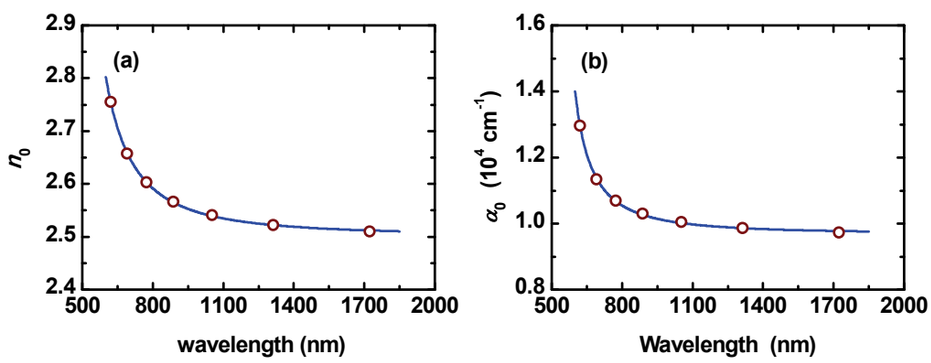

Fig. 5. Wavelength dispersion curve dependence of (a) the linear refractive index and (b) the absorption coefficient of the $BiFeO_3$ thin film. The circles are the calculated data and the solid lines are the theoretical fittings by improved Sellmeier-type formulae.

Figure 5 presents both the linear refractive index n_0 and absorption coefficient α_0 of the $BiFeO_3$ thin film obtained from the transmittance curve using the envelope technique described in subsection 4.1. The circles represent the data obtained by transmittance measurements, which is well fitted to an improved Sellmeier-type dispersion relation (solid lines). As illustrated in Fig. 5(a), the refractive index decreases sharply with increasing wavelength (normal dispersion), suggesting a typical shape of a dispersion curve near an electronic interband transition. At 780 nm, the linear refractive index n_0 and the absorption coefficient α_0 are calculated to be 2.60 and 1.07×10^4 cm^{-1} though the improved Sellmeier-type dispersion fitting (Barboza & Cudney, 2009), respectively. The film thickness calculated in this way is determined to be 510±23 nm.

The optical bandgap of the $BiFeO_3$ film can be estimated using Tauc's formulae $(\alpha_0 h\nu)^{2/m}$=Const.$(h\nu-E_g)$. Although plotting $(\alpha_0 h\nu)^{1/2}$ versus $h\nu$ is illustrated in the insert of Fig. 6, the film is not the indirect bandgap material. From the data shown in Fig. 6, one

obtains m=1 and extrapolates E_g=2.80 eV, indicating that the $BiFeO_3$ ferroelectric has a direct bandgap at 443-nm wavelength. The observation is very close to the reported one prepared by pulse-laser deposition (Kumar et al., 2008). Of course, line and planar defects in the crystalline film and the crystalline size effect could result in a variation of the bandgap. Besides, the bandgap energy also depends on the film processing conditions.

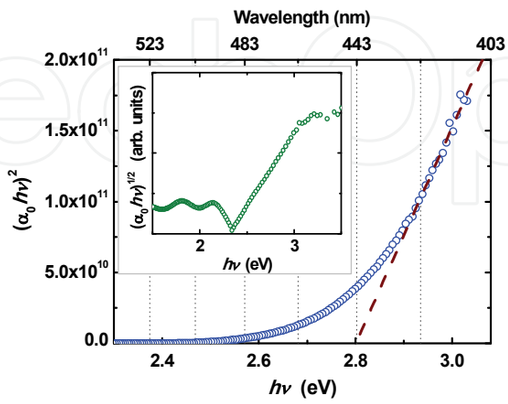

Fig. 6. Plot of $(\alpha_0 h\nu)^2$ versus the photon energy $h\nu$ for the $BiFeO_3$ film. The inset is $(\alpha_0 h\nu)^{1/2}$ versus $h\nu$.

6. Optical nonlinearities of ferroelectric thin films

For the ferroelectric thin films, the large optical nonlinearity is attributed to the small grain size and good homogeneity of the films. During the past two decades, the optical nonlinear response of ferroelectric films has been extensively investigated. In this section, the nonlinear optical properties of some representative ferroelectrics in the nanosecond, picosecond, and femtosecond regimes are presented. Correspondingly, the physical mechanisms are revealed.

6.1 Third-order optical nonlinear properties of ferroelectric films in nanosecond and picosecond regimes

It have been demonstrated that ferroelectric thin films exhibit remarkable optical nonlinearities under the excitation of nanosecond and picosecond laser pulses. Most of these investigations have been mainly performed at λ=532 and 1064 nm (or corresponding the excitation photon energy E_p=2.34 and 1.17 eV). Table 1 summarizes the third-order optical nonlinear coefficients (both n_2 and α_2) of some representative thin films in the nanosecond and picosecond regimes.

The magnitudes of the nonlinear refraction and absorption coefficients in most ferroelectrics at 532 nm are about 10^{-1} cm^2/GW and 10^4 cm/GW, respectively. However, the nonlinear responses of thin films at 1064 nm are much smaller than that at 532 nm. This is due to the nonlinear dispersion and could be interpreted by Kramers-Kronig relations (Boyd, 2009). Interestingly, although the excitation wavelength (λ=1064 nm) for the measurements fulfils the three-photon absorption requirement ($2h\nu<E_g<3h\nu$), the nonlinear absorption processes in undoped and cerium-doped $BaTiO_3$ thin films are the two-photon absorption, which arises from the interaction of the strong laser pulses with intermediate levels in the forbidden gap induced by impurities (Zhang et al., 2000).

As is well known, the optical nonlinearity depends partly on the laser characteristics, in particular, on the laser pulse duration and on the wavelength, and partly on the material itself. As shown in Table 1, the huge difference of both n_2 and α_2 in $CaCu_3Ti_4O_{12}$ thin films with a pulse duration of 25 ps is two orders of magnitude smaller than that with 7 ns (Ning et al., 2009). In what follows, the origin of the observed optical nonlinearity in $CaCu_3Ti_4O_{12}$ films is discussed briefly. As Ning et al. pointed out, the nonlinear absorption mainly originates from the two-photon absorption process because (i) both excitation energy (E_p=2.34 eV) and bandgap (E_g=2.88 eV) of $CaCu_3Ti_4O_{12}$ films fulfil the two-photon absorption requirement ($h\nu<E_g<2h\nu$); and (ii) the free-carrier absorption effect can be negligible because the concentration of free carriers is very low in $CaCu_3Ti_4O_{12}$ films as a high-constant-dielectric material. If the observed nonlinear absorption mainly arises from instantaneous two-photon absorption, the obtained α_2 should be independent of the laser pulse duration, which is quite different from the experimental observations. In fact, the

Films	λ (nm)	n_0	α_0 (cm^{-1})	E_g (eV)	Pulse width	n_2 (cm^2/GW)	α_2 (cm/GW)	References
$CaCu_3Ti_4O_{12}$	532	2.85	4.50×10^4	2.88	7 ns	15.6	4.74×10^5	Ning et al. 2009
$(Ba_{0.7}Sr_{0.3})TiO_3$	532	2.00	1.18×10^4	--	7 ns	0.65	1.20×10^5	Shi et al. 2005
$PbTiO_3$	532	2.34	--	3.50	5 ns	--	4.20×10^4	Ambika et al. 2009
$Pb_{0.5}Sr_{0.5}TiO_3$	532	2.27	--	3.55	5 ns	--	3.50×10^4	Ambika et al. 2009
$PbZr_{0.53}Ti_{0.47}O_3$	532	--	--	3.39	5 ns	--	7.0×10^4	Ambika et al. 2011
$(Pb,La)(Zr,Ti)O_3$	532	2.24	2.80×10^3	3.54	38 ps	-2.26	--	Leng et al. 2007
$SrBi_2Ta_2O_9$	1064	2.25	5.11×10^3	--	38 ps	0.19	--	Zhang et al. 1999
$BaTiO_3$	1064	2.22	3.90×10^3	3.46	38 ps	--	51.7	Zhang et al. 2000
$BaTiO_3$:Ce	1064	2.08	2.44×10^3	3.48	38 ps	--	59.3	Zhang et al. 2000
$Bi_{3.25}La_{0.75}Ti_3O_{12}$	532	2.49	2.46×10^3	3.79	35 ps	0.31	3.0×10^4	Shin et al. 2007
$Bi_{3.75}Nd_{0.25}Ti_3O_{12}$	532	2.01	1.02×10^3	3.56	35 ps	0.94	5.24×10^4	Wang et al. 2004
$Bi_2Nd_2Ti_3O_{12}$	532	2.28	1.95×10^3	4.13	35 ps	0.70	3.10×10^4	Gu et al. 2004
$CaCu_3Ti_4O_{12}$	532	2.85	4.50×10^4	2.88	25 ps	0.13	2.69×10^3	Ning et al. 2009

Table 1. Linear optical parameters and nonlinear optical coefficients of some representative ferroelectric thin films in nanosecond and picosecond regimes.

observed nonlinear absorption mainly originates from the instantaneous two-photon absorption and the accumulative process. As discussed in subsection 3.3, the physical mechanisms of $CaCu_3Ti_4O_{12}$ films can be understood as follows. Under the pulsed excitation of 25 ps, two-photon absorption and population distribution are the main mechanisms of the nonlinear absorption and refraction, respectively. In a few nanosecond time scales, the accumulative absorption (two-step two-photon absorption) and refraction processes by impurities mainly contribute to the nonlinear absorption and refraction effects, respectively.

6.2 Femtosecond third-order optical nonlinearity of polycrystalline $BiFeO_3$

As a new multifunctional material, ferroelectric thin films of $BiFeO_3$ have many notable physical characteristics, such as prominent ferroelectricity, magnetic and electrical properties, and ferroelectric and dielectric characteristics. Besides high optical transparency and excellent optical homogeneity, the $BiFeO_3$ thin films also exhibit remarkable optical nonlinearity (Gu et al., 2009a).

To give an insight into the detailed optical nonlinearities and to identify the corresponding physical mechanisms, the *Z*-scan measurements at different levels of laser intensities I_0 were carried out. To exclude the optical nonlinearity from the substrate, *Z*-scan measurements on a 1.0-mm-thick quartz substrate were also performed. The nonlinear absorption coefficient of α_2^{sub}~0 and the third-order refractive index of n_2^{sub}=3.26×10^{-7} cm^2/GW are extracted from the best fittings between the Z-scan theory for characterizing the instantaneous optical nonlinearity (see subsection 4.2.2) and the experimental data illustrated in Fig. 7(a) at I_0=156 GW/cm^2. The measured n_2^{sub} value is independent of I_0 under our experimental conditions. Figure 7(b) displays typical open- and closed-aperture Z-scan traces for the 510-nm-thick $BiFeO_3$ thin film on the 1.0-mm-thick quartz substrate at I_0=156 GW/cm^2, showing positive signs for both absorptive and refractive nonlinearities, respectively.

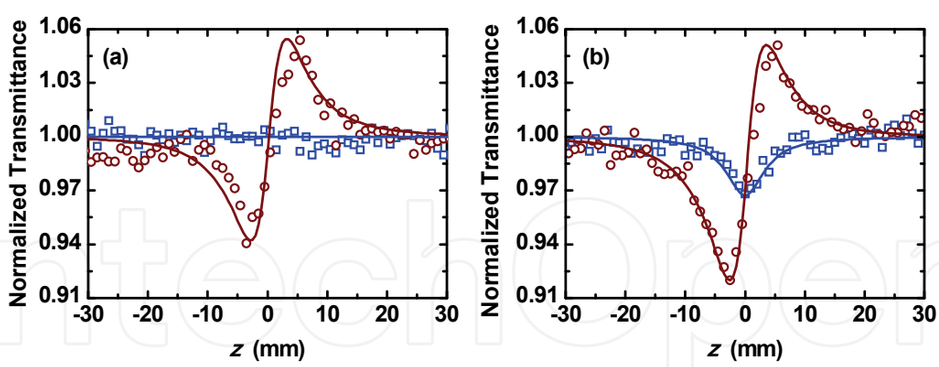

Fig. 7. Examples of Z-scans at I_0 =156 GW/cm^2 for (a) the quartz substrate and (b) the $BiFeO_3$ thin film deposited on the quartz substrate. Squares and circles are the open- and closed-aperture Z-scans, respectively; the solid lines are the best-fit curves calculated by the Z-scan theory.

Rigorous analysis is adopted Z-scan theory for a cascaded nonlinear medium (see subsection 4.2.3). The obtained nonlinear coefficients of α_2 and n_2 for the $BiFeO_3$ thin film at different levels of I_0 display in Fig. 8. Clearly, the values of α_2 and n_2 are independent of the optical intensity, indicating that the observed optical nonlinearities are of cubic nature; and α_2=16.0±0.6 cm/GW and n_2=(1.46±0.06)×10^{-4} cm^2/GW at 780 nm. It should be emphasized

that the above-said nonlinear coefficients are average values due to the polycrystalline, multi-domain nature of the $BiFeO_3$ film.

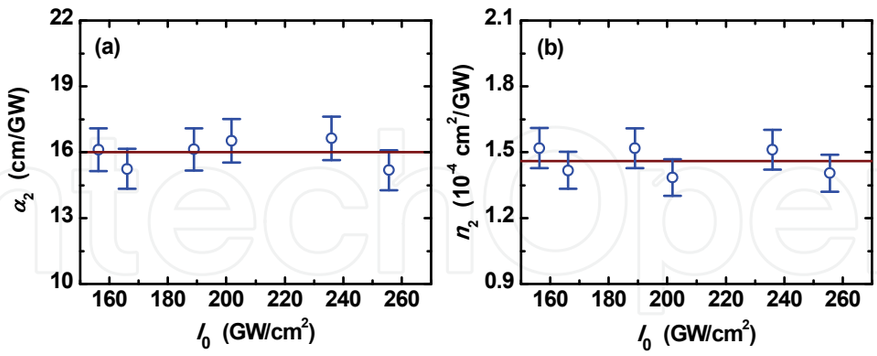

Fig. 8. Intensity independence of (a) nonlinear absorption coefficient α_2 and (b) nonlinear refraction index n_2 for the $BiFeO_3$ thin film, respectively.

The physical mechanisms of the femtosecond optical nonlinearities in the $BiFeO_3$ film can be understood as follows. The positive nonlinear absorption mainly originates from the two-photon absorption process because (i) the Z-scan theory on two-photon absorbers fits open-aperture Z-scan experimental data well; and (ii) both excitation photon energy ($h\nu$=1.60 eV) and bandgap (E_g=2.80 eV) of the $BiFeO_3$ film fulfill the two-photon absorption requirement ($h\nu<E_g<2h\nu$). It is also known that the ultrafast femtosecond pulses can eliminate the contributions to the refractive nonlinearity from optical electrostriction and population redistribution since those effects have a response time much longer than 350 fs. Moreover, accumulative thermal effects are negligible because the experiments were conducted at a low repetition rate of 1 kHz. Consequently, the measured n_2 should directly result from the electronic origin of the refractive nonlinearity in the $BiFeO_3$ thin film.

Films	λ (nm)	n_0	α_0 (cm^{-1})	Eg (eV)	Pulse width	n_2 (cm^2/GW)	α_2 (cm/GW)	References
$Ba_{0.6}Sr_{0.4}TiO_3$	790	2.20	--	3.64	60 fs	6.1×10^{-5}	8.7×10^{-2}	Liu et al. 2006
Bi_3TiNbO_9	800	2.28	1.37×10^{2}	3.40	80 fs	--	1.44×10^{4}	Yang et al. 2009
$Bi_{1.95}La_{1.05}TiNbO_9$	800	2.02	3.04×10^{4}	3.53	100 fs	--	5.95×10^{3}	Chen et al. 2010
$Ba_{0.6}Sr_{0.4}TiO_3$	800	2.25	8.50×10^{3}	3.48	120 fs	3.0×10^{-4}	1.70	Ning et al. 2011
$Bi_{3.25}La_{0.75}Ti_3O_{12}$	800	2.39	1.73×10^{3}	--	140 fs	1.9×10^{-3}	-6.76×10^{-3}	Shi et al. 2006
$BiFeO_3$	780	2.60	1.07×10^{4}	2.80	350 fs	1.5×10^{-4}	16	Gu et al. 2009a
BLFM	780	2.52	5.77×10^{3}	2.90	350 fs	2.0×10^{-4}	7.4	Gu et al. 2009b

Table 2. Linear optical parameters and femtosecond nonlinear optical coefficients of some representative ferroelectric thin films in the near infrared region.

With the proliferation of femtosecond laser systems, the understanding of the ultrafast nonlinear responses of ferroelectric thin films is of direct relevance to both academic interest and technological applications. As such, more and more efforts are concentrated on investigating the femtosecond nonlinear optical properties of ferroelectric films, since the complete understanding of these phenomena is still incomplete. Table 2 summarizes the femtosecond nonlinear optical response of some representative ferroelectric thin films in the near infrared region. The typical value of nonlinear refractive index n_2 is about 10^{-4} cm^2/GW; whereas the nonlinear absorption coefficient α_2 is on a wide range of magnitudes from 10^{-2} to 10^4 cm/GW, depending on both the laser characteristics and on the material itself. In the femtosecond regime, the accumulative effect could be minimized from the contribution of the optical nonlinearity. Thus, the nonlinear absorptive coefficient and refractive index measured with femtosecond laser pulses are closer to the intrinsic value. The electronic Kerr effect and two-photon absorption are the main mechanisms of the third-order nonlinear refraction and absorption, respectively.

6.3 Fifth-order optical nonlinearity in $Bi_{0.9}La_{0.1}Fe_{0.98}Mg_{0.02}O_3$ thin films

The ferroelectric $Bi_{0.9}La_{0.1}Fe_{0.98}Mg_{0.02}O_3$ (BLFM) thin films were deposited on quartz substrates at 650°C by radio frequency magnetron sputtering. The optical transmittance spectrum measurements indicate that the BLFM film has a flat surface, a uniform thickness, and good transparency (Gu et al., 2009b).

The nonlinear optical properties of BLFM films were characterized by the femtosecond Z-scan experiments at different levels of optical intensities I_0. To exclude the optical nonlinear contribution from the substrate, Z-scan measurements on a 1.0-mm-thick quartz substrate were performed. The measured α_2^{sub}~0 and $n_2^{sub}=3.26\times10^{-7}$ cm^2/GW are independent of I_0 within the limit of $I_0\leq270$ GW/cm^2. As examples, for the BLFM thin film deposited on 1.0-mm-thick quartz substrate, typical open- and closed-aperture Z-scans at I_0=156 and 225 GW/cm^2 are shown in Figs. 9(b) and 10(b), respectively. All the open-aperture Z-scans exhibit a symmetric valley with respect to the focus, typical of an induced positive nonlinear absorption effect. Apparently, the observed nonlinear absorption originates from the BLFM thin film only. In the closed-aperture Z-scans, the resultant nonlinear refraction arises from both the BLFM film and the substrate. At a relatively low intensity [see Fig. 9(b)], the closed-aperture Z-scan resembles to the substrate's signal [circles in Fig. 9(a)], suggesting that the nonlinear refraction signal from the BLFM is very weak. Under the excitation of high intensity [see Fig. 10(b)], however, it is noteworthy that the closed-aperture Z-scan displays a much lower peak-to-valley value in contrast with circles in Fig. 10(a), indicating that the BLFM film exhibits a negative nonlinear refraction effect. These facts may imply that both third- and higher-order nonlinearities, rather than a pure third-order process, simultaneously make contributions to the observed signal.

Adopting Z-scan theory for a cascaded nonlinear medium as described in subsection 4.2.3, the effective nonlinear coefficients (both α_{eff} and n_{eff}) of the BLFM film as a function of I_0 are illustrated in Fig. 11. If the film only possesses a cubic nonlinearity in nature, the values of α_{eff} and n_{eff} should be independent on the excitation intensity. As shown in Fig. 11, the values of α_{eff} (or n_{eff}) increases (or decreases) with increasing intensity, suggesting the occurrence of higher-order nonlinear processes. Applying the theory presented in subsection 4.2.4, the measured α_{eff} and n_{eff} values are analyzed. The best fit shown in Fig. 11(a) indicates that α_2=7.4±0.8 cm/GW and α_3 = (8.6±0.6)×10^{-2} cm^3/GW^2. From Fig. 11(b), we obtain n_2=(2.0±1.2)×10^{-4} cm^2/GW and n_4=-(2.4±1.5)×10^{-6} cm^4/GW^2 for the BLFM thin film

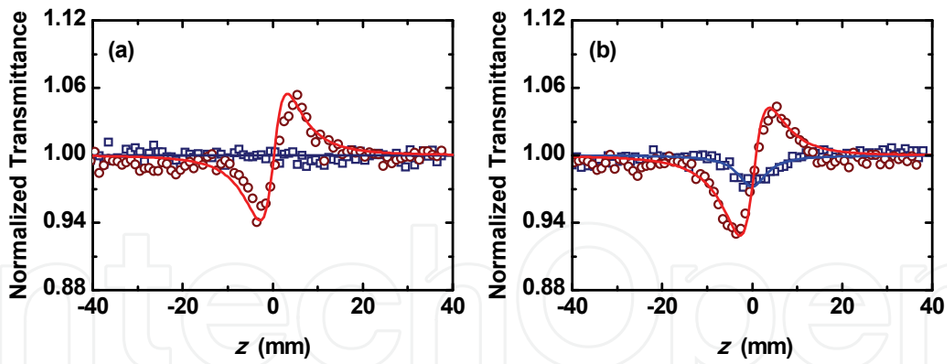

Fig. 9. Examples of Z-scans at I_0=156 GW/cm² for both (a) the quartz substrate and (b) the BLFM thin film deposited on the quartz substrate. Squares and circles are the open- and closed-aperture Z-scans, respectively; while the solid lines are the best-fit curves calculated by the Z-scan theory.

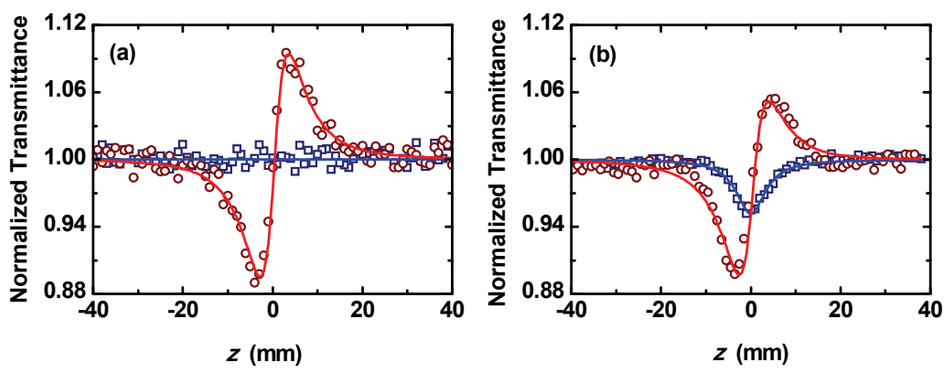

Fig. 10. Examples of Z-scans at I_0=225 GW/cm² for both (a) the quartz substrate and (b) the BLFM thin film deposited on the quartz substrate. Squares and circles are the open- and closed-aperture Z-scans, respectively; while the solid lines are the best-fit curves calculated by the Z-scan theory.

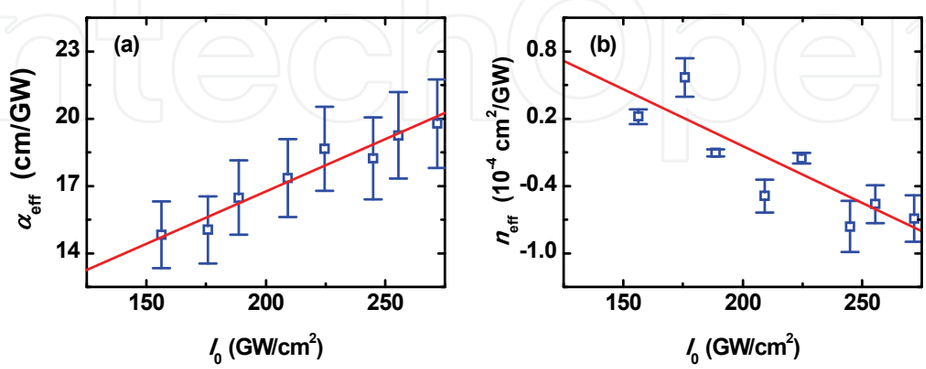

Fig. 11. Intensity dependence of (a) nonlinear absorption coefficient α_{eff} and (b) nonlinear refraction index n_{eff} for the pure BLFM thin film, respectively. The solid lines are for guidance to the eyes.

within the limit of $I_0 \leq 270$ GW/cm^2. Note that in our Z-scan analysis, the intensity change in the film transmission due to the light-induced nonlinear phase in the interference was ignored. This is because that the nonlinear path ($n_{\mathrm{eff}}L_{\mathrm{eff}}I_0$) is estimated to be less than 3% of the wavelength with the parameters mentioned above, and too small to be detectable. For comparison, the obtained n_2 value is three orders of magnitude larger than that of the substrate and is close to that of representative ferroelectric thin films in femtosecond regime as presented in Table 2.

The underlying mechanisms of the optical nonlinearities in the BLFM film are described in the following. As is well known, the nonlinear optical response strongly depends on the laser pulse duration. For instance, the population redistribution is the dominant mechanism of the third-order nonlinear refraction in the ferroelectric thin films in the picosecond regime (Shin et al, 2007). Under the excitation of the femtosecond pulses, the third-order refractive nonlinearity mainly arises from the distortion of the electron cloud. Besides, the accumulative thermal effect is negligible in our experiments because effort was taken to eliminate its contribution by employing ultrashort laser pulses at a low repetition rate (1 kHz in our laser system). Consequently, the measured n_2 gives evidence of the electronic origin of the optical nonlinearity. In addition, the third-order nonlinear absorption is attributed to two-photon absorption because the excitation photon energy ($h\nu$=1.60 eV) and the bandgap (E_g=2.90 eV) of the BLFM films are satisfied with the two-photon absorption requirement ($h\nu < E_g < 2h\nu$).

In general, there are at least two possible mechanisms contributing to the fifth-order nonlinearities: the intrinsic $\chi^{(5)}$ susceptibility and a sequential $\chi^{(3)}$: $\chi^{(1)}$ effect. We believe that the observed fifth-order nonlinearity mainly originates from an equivalent stepwise $\chi^{(3)}$: $\chi^{(1)}$ process because the tendency of the measured coefficients (see Fig. 11) are analogous to those of two-photon-induced excited-state nonlinearities in organic molecules (Gu et al., 2008b) and two-photon-generated free-carrier nonlinearities in semiconductors (Said et al., 1992). The observation can be understood as follows. In the BLFM thin film, the population redistribution assisted by two-photon absorption produces an additional change in both the absorptive coefficient and refractive index, leading to an equivalent stepwise $\chi^{(3)}$: $\chi^{(1)}$ process. Using the theory of two-photon-induced excited-state nonlinearities (Gu et al, 2008b), the absorptive and refractive cross-sections of populated states are estimated to be σ_a=(2.6±0.3)×10^{-17} cm^2 and σ_r=-(0.72±0.46)×10^{-21} cm^3, respectively, from the formulae $\alpha_3=(3\pi)^{1/2}\sigma_a\alpha_2\tau_F/[8(2\ln 2)^{1/2}h\nu]$ and $n_4=(3\pi)^{1/2}\sigma_r\alpha_2\tau_F/[8(2\ln 2)^{1/2}h\nu]$. These values are on the same order of magnitude as the findings for organic molecules (Gu et al., 2008b) and semiconductors (Said et al., 1992), confirming that our inference of the origin of fifth-order effect is reasonable.

7. Summary and prospects

This book chapter describes the linear and femtosecond nonlinear optical properties of ferroelectric thin films. The fundamental optical constants (the linear absorption coefficient, linear refraction index, and bandgap energy) of the thin film are determined by optical transmittance measurements. The nonlinear optical response of the film is characterized by single-beam femtosecond Z-scan technique. The femtosecond third-order optical nonlinearity of polycrystalline $BiFeO_3$ thin film is presented. Moveover, the simultaneous third- and fifth-order nonlinearities in ferroelectric $Bi_{0.9}La_{0.1}Fe_{0.98}Mg_{0.02}O_3$ films are observed. Most importantly, the nonlinear optical properties of representative ferroelectric thin films in nanosecond, picosecond, and femtosecond regimes are summarized. The underlying mechanisms for the optical nonlinearities of ferroelectric thin films are discussed in details.

In literature, the optical nonlinearity will be enhanced by the dielectric and local field effect as well as the homogeneity in diameter, distribution and orientation in the ferroelectric films (Ruan et al., 2008). Researchers found that the nonlinear optical properties of ferroelectric films are also dependent on both fabrication techniques and deposited temperature (Saravanan et al., 2010). The ions (Pb, Mn, or K) dopant as the acceptor in ferroelectric films could reduce the dielectric loss and enhance the third-order optical nonlinearity (Zhang et al., 2008, Ning et al., 2011). By altering the lattice defect and subsequent the density of intermediate energy states, it is possible to tune the optical nonlinear response of ferroelectric thin films (Ambika et al., 2011). Metal nanoparticles doped ferroelectrics will introduce additional absorption peak arising from the surface plasmon resonance of nanoparticles. Accordingly, one could detect the huge enhancement of the near resonance nonlinearity in ferroelectric composite films (Chen et al., 2009). Besides, novel ferroelectric hybrid compounds, such as ferroelectric inorganic-organic hybrids, show the high thermal stability, insolubility in common solvents and water, and wide transparency range, which make them potential candidates for nonlinear photon devices (Zhao et al., 2009).

8. Acknowledgments

We acknowledge financial support from the National Science Foundation of China (Grant Number: 10704042) and the program for New Century Excellent Talents in University.

9. References

Ambika, D.; Kumar, V.; Sandeep, C. S. S. & Philip, R. (2009). Non-linear optical properties of $(Pb_{1-x}Sr_x)TiO_3$ thin films. *Applied Physics B – Lasers and Optics*, 97, 3 (Nov): 661-664.

Ambika, D.; Kumar, V.; Sandeep, C. S. S. & Philip, R. (2011). Tunability of third order nonlinear absorption in $(Pb,La)(Zr,Ti)O_3$ thin films. *Applied Physics Letters*, 98, 1 (Jan): 011903.

Barboza, N. A. & Cudney, R. S. (2009). Improved Sellmeier equation for congruently grown lithium tantalate. *Applied Physics B – Lasers and Optics*, 95, 3 (Jun): 453-458.

Boyd, R. W. (2009). *Nonlinear Optics*, Elsevier Inc., 978-981-272480-9 Singapore.

Chen, K. S.; Gu, H. S.; Cai, Y. X.; Xiong, J. & Wang, A. M. (2009). $Fe/SrBi_2Nb_2O_9$ composite thin films with large third-order optical nonlinearities. *Journal of Alloys and Compounds*, 476, 1-2 (May): 635-638.

Chen, H. Z.; Yang, B.; Zhang, M. F.; Wang, F. Y.; Cheah, K. & Cao, W. W. (2010). Third-order optical nonlinear absorption in $Bi_{1.95}La_{1.05}TiNbO_9$ thin films. *Thin Solid Films,* 518, 19 (Jul): 5585-5587.

Chen, Y. F.; Beckwitt, K.; Wise, F. W.; Aitken, B. G.; Sanghera, J. S. & Aggarwal, I. D. (2006). Measurement of fifth- and seventh-order nonlinearities of glasses. *Journal of the Optical Society of American B – Optical Physics*, 23, 2 (Feb): 347-352.

DiDomenico, M. & Wemple, S. H. (1969). Oxygen-octahedra ferroelectrics. I. Theory of electro-optical and nonlinear optical effects. *Journal of Applied Physics*, 40, 2 (Feb): 720-734.

Gu, B.; Wang, Y. H.; Peng, X. C.; Ding, J. P.; He, J. L. & Wang, H. T. (2004). Giant optical nonlinearity of a $Bi_2Nd_2Ti_3O_{12}$ ferroelectric thin film. *Applied Physics Letters*, 85, 17(Oct): 3687-3689.

Gu, B.; Ji, W. & Huang, X. Q. (2008a). Analytical expression for femtosecond-pulsed z scans on instantaneous nonlinearity. *Applied Optics*, 47, 9 (Mar): 1187-1192.

Gu, B.; Sun, Y. & Ji, W. (2008b). Two-photon-induced excited-state nonlinearities. *Optics Express*, 16, 22 (Oct): 17745-17751.

Gu, B.; Wang, Y.; Wang, J. & Ji, W. (2009a). Femtosecond third-order optical nonlinearity of polycrystalline $BiFeO_3$. *Optics Express*, 17, 13(June): 10970-10975.

Gu, B.; Wang, Y.; Ji, W. & Wang, J. (2009b). Observation of a fifth-order optical nonlinearity in $Bi_{0.9}La_{0.1}Fe_{0.98}Mg_{0.02}O_3$ ferroelectric thin films. *Applied Physics Letters*, 95, 4(Aug): 041114.

Gu, B.; Lou, K.; Chen, J.; Li, Y. N.; Wang, H. T. & Ji. W. (2010). Excited-state enhancement of third-order optical nonlinearities: photodynamics and characterization. *Optics Express*, 18, 26 (Dec): 26843-26853.

Kityk, A. V.; Czaplicki, R.; Klöpperpieper, A.; Andrushchak, A. S. & Sahraoui, B. (2010). Spontaneous and electric field induced quadratic optical nonlinearity in ferroelectric crystals $AgNa(NO_2)_2$. *Applied Physics Letters*, 96, 6 (Feb): 061911.

Kumar, A.; Rai, R. C.; Podraza, N. J.; Denev, S.; Ramirez, M.; Chu, Y. H.; Martin, L. W.; Ihlefeld, J.; Heeg, T.; Schubert, J.; Schlom, D. G.; Orenstein. J.; Ramesh, R.; Collins, R. W.; Musfeldt, J. L. & Gopalan, V. (2008). Linear and nonlinear optical properties of $BiFeO_3$. *Applied Physics Letters*, 92, 12 (Mar): 121915.

Leng, W. J.; Yang, C. R.; Ji, H.; Zhang, J. H.; Tang, J. L.; Chen, H. W. & Gao, L. F. (2007). Linear and nonlinear optical properties of (Pb, La)(Zr, Ti)O_3 ferroelectric thin films grown by radio-frequency magnetron sputtering. *Journal of Physics D – Applied Physics*, 40, 4 (Feb): 1206-1210.

Liu, S. W.; Xu, J.; Guzun, D.; Salamo, G. J.; Chen, C. L.; Lin, Y. & Xiao, M. (2006). Nonlinear optical absorption and refraction of epitaxial $Ba_{0.6}Sr_{0.4}TiO_3$ thin films on (001) MgO substrates. *Applied Physics B-Lasers and Optics*, 82, 3(Mar): 443-447.

Murgan, R.; Tilley, D. R.; Ishibashi, Y.; Webb, J. F. & Osman, J. (2002). Calculation of nonlinear-susceptibility tensor components in ferroelectrics: cubic, tetragonal, and rhombohedral symmetries. *Journal of the Optical Society of American B – Optical Physics*, 19, 9 (Sep): 2007-2021.

Ning, T. Y.; Chen, C.; Zhou, Y. L.; Lu, H.; Zhang, D. X.; Ming, H. & Yang, G. Z. (2009). Larger optical nonlinearity in $CaCu_3Ti_4O_{12}$ thin films. *Applied Physics A – Materials Science & Processing,* 94, 3 (Mar): 567-570.

Ning, T. Y.; Chen, C.; Wang, C.; Zhou, Y. L.; Zhang, D. X.; Ming, H. & Yang, G. Z. (2011). Enhanced femtosecond optical nonlinearity of Mn doped $Ba_{0.6}Sr_{0.4}TiO_3$ films. *Journal of Applied Physics*, 109, 1 (Jan): 013101.

Ruan, K. B.; Gao, A. M.; Deng, W. L.; Chen, X. M. & Bao, D. (2008). Orientation dependent photoluminescent properties of chemical solution derived $Bi_{4-x}Eu_xTi_3O_{12}$ ferroelectric thin films. *Journal of Applied Physics*, 104, 3 (Aug): 036101.

Said, A. A.; Sheik-Bahae, M.; Hagan, D. J.; Wei, T. H.; Wang, J. & Van Stryland, E. W. (1992). Determination of bound-electronic and free-carrier nonlinearities in ZnSe, GaAs, CdTe, and ZnTe. *Journal of the Optical Society of American B – Optical Physics*, 9, 3 (Mar): 405-414.

Saravanan, K. V.; Raju, K. C. J.; Krishna, M. G.; Tewari, S. P. & Rao, S. V. (2010). Large three-photon absorption in $Ba_{0.5}Sr_{0.5}TiO_3$ films studied using Z-scan technique. *Applied Physics Letters*, 96, 23(Jun): 232905.

Sheik-Bahae, M; Said, A. A.; Wei, T. H.; Hagan, D. J. & Van Stryland, E. W. (1990). Sensitive measurement of optical nonlinearities using a single beam. *IEEE Journal of Quantum Electronics*, 26, 4(Apr): 760-769.

Shi, F. W.; Meng, X. J.; Wang, G. S.; Sun, J. L; Lin, T.; Ma, J. H.; Li, Y. W. & Chu, J. H. (2006). The third-order optical nonlinearity of $Bi_{3.25}La_{0.75}Ti_3O_{12}$ ferroelectric thin film on quartz. *Thin Solid Films*, 496, 2 (Feb): 333-335.

Shi, P.; Yao, X.; Zhang, L. Y.; Wu, X. Q.; Wang, M. Q. & Wan, X. (2005). Third-order optical nonlinearity of $(Ba_{0.7}Sr_{0.3})TiO_3$ ferroelectric thin films fabricated by soft solution processing. *Soild State Communications*, 134, 9 (Jun): 589-593.

Shin, H.; Chang, H. C.; Boyd, R. W.; Choi, M. R. & Jo, W. (2007). Large nonlinear optical response of polycrystalline $Bi_{3.25}La_{0.75}Ti_3O_{12}$ ferroelectric thin films on quartz substrates. *Optics Letters*, 32, 16 (Aug): 2453-2455.

Swanepoel, R. (1983). Determination of the thickness and optical constants of amorphous silicon. *Journal of Physics E: Scientific Instruments*, 16, 12 (Dec): 1214-1222.

Tauc, J.; Gigorovici, R. & Vancu, A. (1966). Optical properties and electronic structure of amorphous germanium. *Physica Status Solidi B*, 15, 2 (Mar): 627-637.

Tsai, C. A.; Wu, A. Y.; Liou, W. R. & Lin, W. C. (2004). Second harmonic generation in Barium Titanate thin films on silica glass by corona poling. *Japanese Journal of Applied Physics*, 43, 4A (Apr): 1348-1356.

Wang, Y. H.; Gu, B.; Xu, G. D. & Zhu, Y. Y. (2004). Nonlinear optical properties of neodymium-doped bismuth titanate thin films using Z-scan technique. *Applied Physics Letters*, 84, 10 (Mar): 1686-1688.

Yang, B; Chen, H. Z.; Zhang, M. F.; Wang, F. Y.; Cheah, K. & Cao. W. W. (2009). Nonlinear optical absorption in Bi_3TiNbO_9 thin films using Z-scan technique. *Applied Physics A – Materials Science & Processing,* 96, 4 (Sep): 1017-1021.

Zang, W. P.; Tian, J. G.; Liu, Z. B.; Zhou, W. Y.; Zhang, C. P. & Zhang, G. Y. (2003). Study on Z-scan characterisitics of cascaded nonlinear media. *Applied Physics B-Lasers and Optics*, 77, 5(Oct): 529-533.

Zhang, T.; Zhang, W. F.; Chen. Y. H. & Yin. J. (2008). Third-order optical nonlinearities of lead-free $(Na_{1-x}K_x)_{0.5}Bi_{0.5}TiO_3$ thin films. *Optics Communications*, 281, 3(Feb): 439-443.

Zhang, W. F.; Zhang, M. S.; Yin, Z.; Gu, Y. Z.; Du, Z. L. & Yu, B. L. (1999). Large third-order optical nonlinearity in $SrBi_2Ta_2O_9$ thin films. *Applied Physics Letters*, 95, 7(Aug): 902-904.

Zhang, W. F.; Huang, Y. B.; Zhang, M. S. & Liu, Z. G. (2000). Nonlinear optical absorption in undoped and cerium-doped $BaTiO_3$ thin films using Z-scan technique. *Applied Physics Letters*,76, 8(Feb): 1003-1005.

Zhao, H. R.; Li, D. P.; Ren, X. M.; Song, Y. & Jin, W. Q. (2009). Larger spontaneous polarization ferroelectric inorganic-organic hybrids: $[PbI_3]_\infty$ chains directed organic cations aggregation to Kagomé-shaped tubular architecture. *Journal of the American Chemical Society,* 132, 1 (Jan): 18-+.

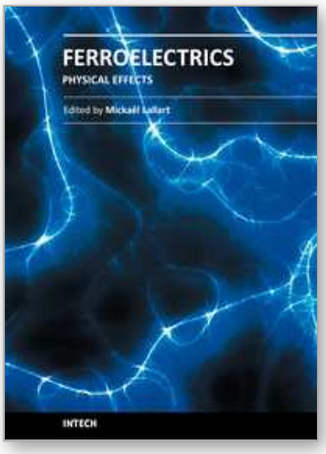

Ferroelectrics - Physical Effects

Edited by Dr. MickaÃ«l Lallart

ISBN 978-953-307-453-5
Hard cover, 654 pages
Publisher InTech
Published online 23, August, 2011
Published in print edition August, 2011

Ferroelectric materials have been and still are widely used in many applications, that have moved from sonar towards breakthrough technologies such as memories or optical devices. This book is a part of a four volume collection (covering material aspects, physical effects, characterization and modeling, and applications) and focuses on the underlying mechanisms of ferroelectric materials, including general ferroelectric effect, piezoelectricity, optical properties, and multiferroic and magnetoelectric devices. The aim of this book is to provide an up-to-date review of recent scientific findings and recent advances in the field of ferroelectric systems, allowing a deep understanding of the physical aspect of ferroelectricity.

InTech Europe
University Campus STeP Ri
Slavka Krautzeka 83/A
51000 Rijeka, Croatia
Phone: +385 (51) 770 447
Fax: +385 (51) 686 166
www.intechopen.com

InTech China
Unit 405, Office Block, Hotel Equatorial Shanghai
No.65, Yan An Road (West), Shanghai, 200040, China
中国上海市延安西路65号上海国际贵都大饭店办公楼405单元
Phone: +86-21-62489820
Fax: +86-21-62489821